ACS APPLIED MATERIALS & INTERFACES

Research Article

www.acsami.org

Amorphous Thieno[3,2-*b*]thiophene and Benzothiadiazole Based Copolymers for Organic Photovoltaics

Wonho Lee,[†,§] Hyojung Cha,[‡,§] Yu Jin Kim,[‡] Ji-Eun Jeong,[†] Sungu Hwang,[∥] Chan Eon Park,*[,‡] and Han Young Woo*[,†]

[†]Department of Nanofusion Engineering, Department of Cogno-Mechatronics Engineering, and [∥]Department of Nanomechatronics Engineering, Pusan National University, Miryang, Gyeongsangnam-do 627-706, Republic of Korea

[‡]POSTECH Organic Electronics Laboratory, Department of Chemical Engineering, Pohang University of Science and Technology, Pohang, 790-784, Republic of Korea

Supporting Information

ABSTRACT: Three types of amorphous thienothiophene (TT)-benzothiadiazole (BT) based copolymers (**PFTTBT**) were synthesized by incorporating alkyl-substituted fluorene moieties as a third component in the polymer backbone. Their optical, electrochemical, morphological, and photovoltaic properties were examined by a comparison with those of a crystalline TT-BT derivative (**PTTBT14**). **PTTBT14** was reported to have a high hole mobility (0.26 $cm^2/(V\ s)$) due to the pronounced interchain ordering but poor photovoltaic power conversion efficiency (PCE) of 2.4−2.6% was reported due to excessively strong self-interactions with poor miscibility with fullerene structures. By incorporating fluorene units, the UV−vis spectra showed an increased bandgap (~1.9 eV) with the disappearance of the packing-originated shoulder peak, and the valence band decreased compared to crystalline **PTTBT14**. The amorphous **PFTTBT** polymers showed substantially improved photovoltaic properties compared to **PTTBT14**, even though they showed poor hole mobility ($\sim 10^{-6}$ $cm^2/(V\ s)$) and fill factor. The optimal devices were achieved by blending with excess $PC_{71}BM$ (polymer:$PC_{71}BM$ = 1:4 by weight), showing little improvement in the thermal and additive treatments. Under simulated solar illumination of AM 1.5 G, the best PCE of 6.6% was achieved for a **PFehTTBT**:$PC_{71}BM$ device with an open-circuit voltage of 0.92 V, a short-circuit current of 15.1 mA/cm^2, and a fill factor of 0.48. These results suggest that it is useful to disrupt partially the interchain organizations of excessively crystalline polymers, enabling fine-control of intermolecular ordering and the morphological properties (i.e., miscibility with fullerene derivatives, etc.) to utilize the advantages of both crystalline and amorphous materials for further improving PCE of polymer solar cells.

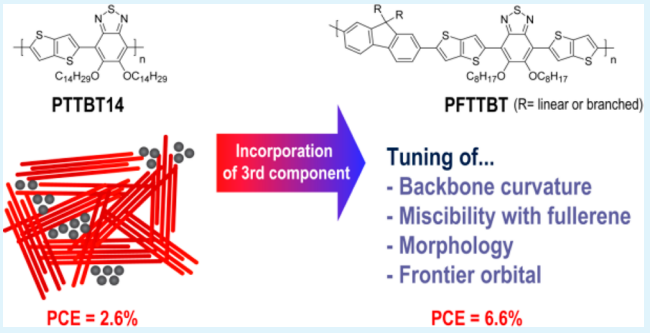

KEYWORDS: *conjugated polymer, polymer solar cells, photovoltaic polymer, fluorene, noncovalent coulomb interaction*

INTRODUCTION

Recently, organic photovoltaics (OPVs) have attracted increasing attention from both academia and industry because of their lightweight, mechanical flexibility, and low-cost large-area solution processing.[1−5] A bulk heterojunction (BHJ) OPV system is composed of a photoactive blended layer of an electron-donating conjugated polymer and an electron-accepting fullerene derivative between the transparent anode and highly reflective cathode. Over the past decade, several studies on molecular design and device optimization have led to rapid improvement in the power conversion efficiency (PCE) of OPVs, showing more than 9% in a single cell device architecture.[6−11] An ideal polymeric semiconductor should possess broad absorption to harvest more sunlight to achieve a higher short circuit current (J_{SC}), deep highest occupied molecular orbital (HOMO) level to maximize the open circuit voltage (V_{OC}), while keeping the proper lowest unoccupied molecular orbital (LUMO) level for efficient electron transfer to the fullerene-based acceptors, and high hole mobility to increase J_{SC} and fill factor (FF). In addition, the molecular weight and nanoscale film morphology also need to be optimized to improve the PCEs. Donor−acceptor (D−A) alternating copolymers suggest a very useful strategy to control the above issues.[12,13] On the other hand, examining D−A copolymers with new donor or acceptor structures for clarifying the structure−property relationships and maximizing the device performance of OPVs is still a challenge.

A recent study reported a thienothiophene (TT) and benzothiadiazole (BT) based low bandgap copolymer, poly-(5,6-bis(tetradecyloxy)-4-(thieno[3,2-*b*]thiophene-2-yl)benzo-

Received: September 8, 2014
Accepted: October 22, 2014
Published: October 22, 2014

[c][1,2,5]thiadiazole) (**PTTBT14**) with a linear and planar main backbone, showing highly crystalline interchain organization via intra- and/or intermolecular hydrogen bonds and S (δ^+)···O (δ^-) dipole−dipole interactions with the resulting efficient charge transport (hole mobility, 0.26 $cm^2/(V\ s)$).[14] The TT moiety has more extended π-orbital delocalization than thiophene, and its linear bond angle gives rise to strong intermolecular interaction with the resulting crystalline morphology.[15,16] **PTTBT14** exhibited pronounced intermolecular packing characteristics, showing well-resolved interlamellar scattering peaks up to (300) with a strong edge-on orientation in the two-dimensional grazing incidence wide-angle X-ray scattering (GIWAXS) measurements. D−A type alternating copolymers normally show poor crystalline ordering compared to P3HT even after thermal annealing. The fine-tuning of noncovalent coulomb interactions and chain curvature in the molecular design has proven to be quite effective in controlling the resulting crystalline film morphology.[17−21] On the other hand, crystalline **PTTBT14** showed poor photovoltaic properties by blending with [6,6]-phenyl-C_{61}-butyric acid methyl ester ($PC_{61}BM$), showing 2.4−2.6% PCE due to the excessively strong self-interaction and little miscibility with $PC_{61}BM$. In addition, the high polymer crystallinity increases charge carrier mobility but may lead to slow charge separation due to coarse phase segregation and formation of the interchain excited states from which the charge separation is not energetically favorable.[22] This emphasizes that the highly crystalline polymer (with a high hole mobility) does not always guarantee high-level photovoltaic properties with the desired morphology with fullerene acceptors.[14] It is very important to finely control the crystalline (or amorphous) nature of photoactive polymers for fine adjustments of each photovoltaic parameter for maximization of energy conversion efficiency.

In this study, the molecular structure of **PTTBT14** was modified to decrease its chain linearity and crystalline nature by incorporating a fluorene unit as a third component in the polymeric backbone. Three types of amorphous TT-BT based conjugated polymers were synthesized by varying the alkyl substituents on the 9-position of fluorene with octyl (**PF8TTBT**), 3,7-dimethyloctyl (**PF10TTBT**), and 2-ethylhexyl (**PFehTTBT**) moieties. The incorporation of an alkyl-substituted fluorene moiety increases the solution solubility substantially but decreases the interchain packing interactions significantly. These polymers clearly exhibit amorphous characteristics and poor hole mobility ($\sim 10^{-6}$ $cm^2/(V\ s)$) in contrast to **PTTBT14**, but remarkably improved photovoltaic properties were measured. **PFehTTBT** showed a maximum PCE of 6.6% with a V_{OC} of 0.92 V, J_{SC} of 15.1 mA/cm^2, and FF of 0.48 by blending with [6,6]-phenyl-C_{71}-butyric acid methyl ester ($PC_{71}BM$). The optical, electrochemical, morphological, and the resulting photovoltaic properties of the amorphous TT-BT polymers will be discussed by a comparison with the characteristics of crystalline **PTTBT14**.

EXPERIMENTAL SECTION

Materials. All chemical reagents were purchased from Aldrich Co., Junsei Chemical Co., and TCI and used without further purification. 2,7-Bis(4,4,5,5,-tetramethyl-1,3,2-dioxaborolan-2-yl)-9,9-dioctylfluorene (5a), 2,7-bis(4,4,5,5,-tetramethyl-1,3,2-dioxaborolan-2-yl)-9,9-bis(3,7-dimethyloctyl)fluorene (5b), 2,7-bis(4,4,5,5,-tetramethyl-1,3,2-dioxaborolan-2-yl)-9,9-bis(2-ethylhexyl)fluorene (5c), and 4,7-dibromo-5,6-bis(octyloxy)benzo[c][1,2,5]thiadiazole (1) were synthesized according to previously reported procedures.[19,23]

Hole and Electron Mobility Measurement. Hole-only and electron-only devices of the polymers were fabricated with a configuration of ITO/PEDOT:PSS/polymer:$PC_{71}BM$/Au and Al/polymer:$PC_{71}BM$/Al. The polymer:$PC_{71}BM$ devices were prepared in a similar way to those mentioned in the PSCs fabrication (polymer:$PC_{71}BM$ = 1:4 wt % in *o*-dichlorobenzene). The charge carrier mobilities for blend films were measured by the space charge limited current (SCLC) method.[24]

Synthesis. *2-(Trimethylstannyl)thieno[3,2-b]thiophene (2).* Into a stirred solution of thieno[3,2-*b*]thiophene (0.35 g, 2.5 mmol) in dry tetrahydrofuran (THF, 10 mL) was slowly added *n*-BuLi in hexane (2.5 M, 1 mL, 2.5 mmol) at −78 °C. After being stirred for 1 h, trimethyltin chloride in THF (1 M, 2.5 mL, 2.5 mmol) was added to the reaction mixture and the resulting solution was allowed to warm to room temperature with stirring for 4 h. The reaction mixture was quenched with adding water. The extracted organic phase was dried over anhydrous $MgSO_4$. A dark oil-like compound was obtained after evaporating solvents. The product was used for the next step without purification. Yield: 0.52 g (68%). ^{1}H NMR (300 MHz, $CDCl_3$): δ (ppm) 7.35 (d, 1H), 7.28 (s, 1H), 7.23 (d, 1H), 0.38 (s, 9H). ^{13}C NMR (75 MHz, $CDCl_3$): δ (ppm) 145.11, 141.46, 141.13, 127.17, 126.33, 118.92, −8.23.

4,7-Bis(thieno[3,2-b]thiophene-2-yl)-5,6-bis(octyloxy)benzo[c][1,2,5]thiadiazole (3). 2-(Trimethylstannyl)thieno[3,2-*b*]thiophene (0.51 g, 1.7 mmol), 4,7-dibromo-5,6-bis(octyloxy)benzo[*c*][1,2,5]-thiadiazole (1) (0.37 g, 0.67 mmol), and $Pd(PPh_3)_4$ (3 mol %) were dissolved in dry *N*,*N*-dimethyformamide (DMF, 10 mL). The reaction mixture was refluxed for 12 h under nitrogen. After cooling to room temperature, water was added and the organic layer was separated by extraction with dichloromethane (DCM). The extracted organic layer was washed with brine and dried over anhydrous $MgSO_4$. The solvent was evaporated and the product was purified by column chromatography (eluent, hexane:DCM = 5:1, v:v). Yield: 0.37 g (82%). ^{1}H NMR (300 MHz, $CDCl_3$): δ (ppm) 8.82 (s, 2H), 7.48 (d, 2H), 7.35 (d, 2H), 4.17 (t, 4H), 1.98−1.94 (m, 4H), 1.50−1.28 (m, 20H), 0.88 (t, 6H). ^{13}C NMR (75 MHz, $CDCl_3$): δ (ppm) 151.89, 150.77, 141.36, 139.28, 137.27, 128.22, 122.93, 119.36, 117.98, 74.66, 31.80, 30.36, 29.51, 29.28, 25.96, 22.66, 14.10. Elemental analysis calcd for $C_{34}H_{40}N_2O_2S_5$: C, 61.04; H, 6.03; N, 4.19; S, 23.96. Found: C, 61.13; H, 6.04; N, 4.05; S, 24.08.

4,7-Bis(5-bromothieno[3,2-b]thiophene-2-yl)-5,6-bis(octyloxy)-benzo[c][1,2,5]thiadiazole (4). Into a stirred solution of compound 3 (0.46 g, 0.69 mmol) in DMF (20 mL) was added *N*-bromosuccinimide (0.26 g, 1.4 mmol). The reaction mixture was stirred at room temperature for 2 h and washed with saturated brine. The organic solution was dried over anhydrous $MgSO_4$. The solvent was evaporated and the product was purified by column chromatography (eluent, hexane:DCM = 5:1, v:v). Yield: 0.51 g (90%). ^{1}H NMR (300 MHz, $CDCl_3$): δ (ppm) 8.74 (s, 2H), 7.33 (s, 2H), 4.17 (t, 4H), 1.98−1.94 (m, 4H), 1.50−1.28 (m, 20H), 0.89 (t, 6H). ^{13}C NMR (75 MHz, $CDCl_3$): δ (ppm) 151.80, 150.59, 140.19, 139.47, 135.59, 122.47, 122.19, 117.73, 114.66, 74.76, 31.82, 30.34, 29.50, 29.29, 25.95, 22.68, 14.11. Elemental analysis calcd for $C_{34}H_{38}Br_2N_2O_2S_5$: C, 49.39; H, 4.63; N, 3.39; S, 19.39. Found: C, 49.65; H, 4.71; N, 3.28; S, 20.02.

General Polymerization Procedure. 4,7-Bis(5-bromothieno[3,2-*b*]thiophene-2-yl)-5,6-bis(octyloxy)benzo[*c*][1,2,5]thiadiazole (0.25 g, 0.30 mmol), fluorene monomer (5a, 5b, or 5c, 0.30 mmol), and $Pd(PPh_3)_4$ (3 mol %) were dissolved in a mixture of degassed toluene (10 mL) and aqueous 2 M K_2CO_3 solution (4 mL). The reaction mixture was stirred at 90 °C for 24 h. After the reaction was completed, bromobenzene (0.5 equiv) was added as an end-capper. After 2 h, phenylboronic acid (1.0 equiv) was added and the mixture was further reacted overnight. The resulting reaction solution was precipitated into methanol, and the crude polymers were purified by Soxhlet extraction with acetone, hexane, and chloroform successively. The dissolved chloroform fraction was precipitated into methanol and dried under vacuum at 50 °C.

PF8TTBT. Yield: 249 mg (78%). ^{1}H NMR (300 MHz, $CDCl_3$): δ (ppm) 8.78−8.50 (br, 2H), 7.83−7.44 (br, 6H), 4.40−4.10 (m, 4H),

Scheme 1. (a) Synthetic Routes to PFTTBT Polymers and (b) Molecular Structures

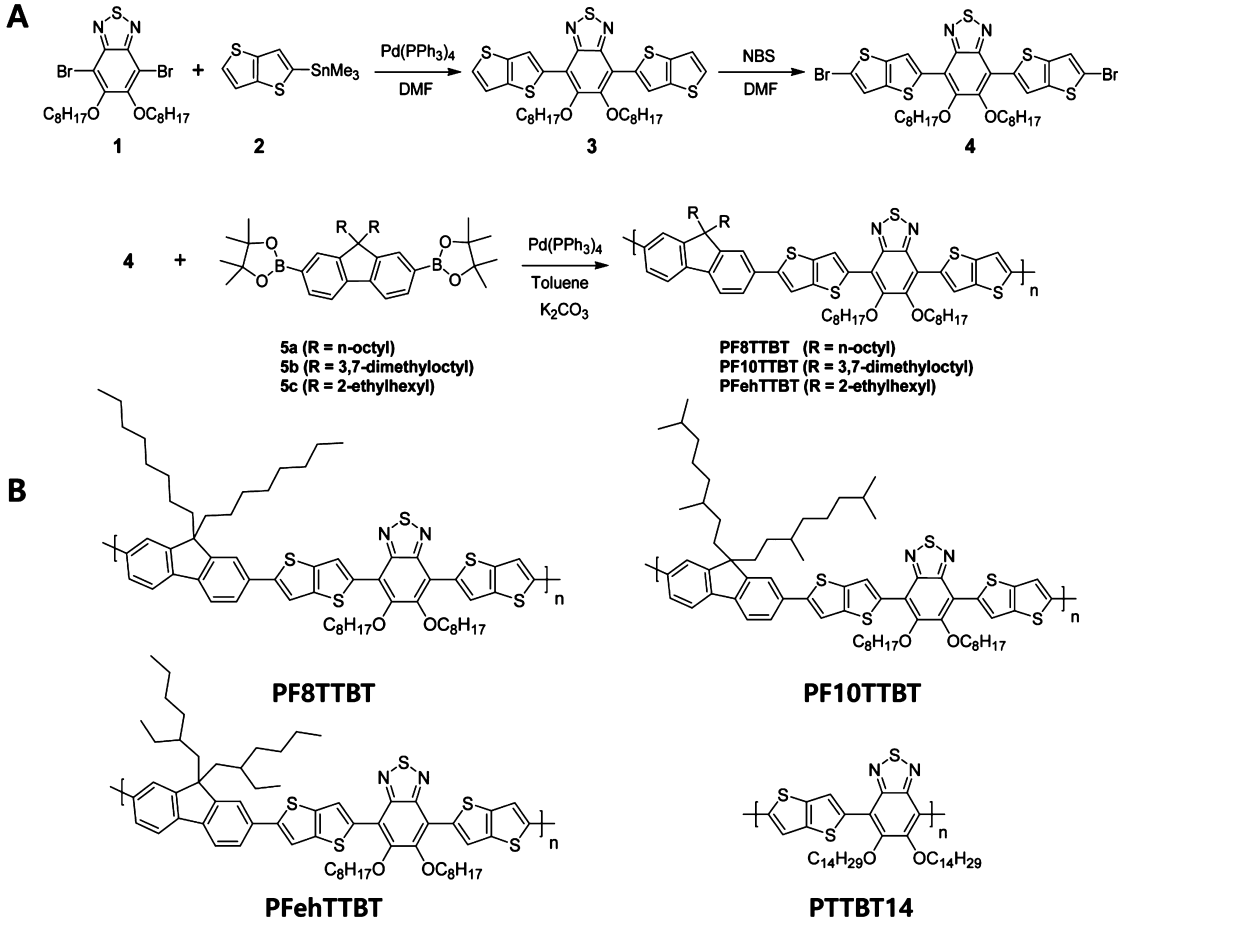

2.07 (m, 8H), 1.58−1.20 (m, 44H), 0.92−0.79 (br, 12H). Number-average molecular weight (by GPC with $CHCl_3$), M_n = 34 000 g mol^{-1} (PDI = 2.8).

PF10TTBT. Yield: 168 mg (50%). ^{1}H NMR (300 MHz, $CDCl_3$): δ (ppm) 8.88−8.75 (br, 2H), 7.83−7.50 (br, 6H), 4.40−4.10 (m, 4H), 2.04 (m, 8H), 1.58−0.50 (br, 64H). M_n = 44 000 g mol^{-1} (PDI = 2.5).

PFehTTBT. . Yield: 255 mg (80%). ^{1}H NMR (300 MHz, $CDCl_3$): δ (ppm) 8.86 (s, 2H), 7.83−7.50 (br, 6H), 4.40−4.10 (m, 4H), 2.03 (m, 8H), 1.58−1.20 (m, 38H), 0.92−0.55 (br, 18H). M_n = 34 000 g mol^{-1} (PDI = 2.3).

RESULTS AND DISCUSSION

Synthesis and Characterization. Scheme 1 outlines the synthetic routes to the monomers and polymers. 4,7-Dibromo-5,6-bis(octyloxy)benzo[*c*][1,2,5]thiadiazole (1) and boronic-esters of alkyl-substituted fluorene (alkyl group: octyl (5a), 3,7-diemthyloctyl (5b), and 2-ethylhexyl (5c)) were synthesized using the previously proposed procedures.[19,23] Monomer 4 was synthesized by Stille-coupling between compounds 1 and 2 in 82% yield and a successive bromination reaction with *N*-bromosuccinimide in 90% yield. To examine the effects of alkyl substituents on the photophysical properties, linear (octyl) and branched (3,7-dimethyloctyl or 2-ethylhexyl) alkyl side chains were introduced onto the 9-position of fluorene. Additional octyloxy substituents were also incorporated onto the electron-deficient (e-deficient) BT unit to increase the solubility. For all structures, there are no alkyl side chains on the electron-rich (e-rich) thienothiophene moiety, which does not increase the HOMO level of the polymers by alkyl substitution. Polymerization was performed by Suzuki−Miyaura coupling between the boronic-ester monomers 5 and brominated monomer 4 in a mixture of toluene and aqueous 2 M K_2CO_3 with $Pd(PPh_3)_4$ as a catalyst. The polymers were purified by Soxhlet extraction (solvent: acetone, hexane, and chloroform) to remove the byproducts and oligomers. The polymers were obtained as a dark red solid in 50−80% yield and were readily soluble in common organic solvents, such as toluene, chloroform, and chlorobenzene, etc. The molecular weight and molecular weight distribution were determined to be 34 000 g/mol (polydispersity index (PDI) = 2.8) for **PF8TTBT**, 44 000 g/mol (PDI = 2.5) for **PF10TTBT**, and 34 000 g/mol (PDI = 2.3) for **PFehTTBT**, respectively, by GPC using chloroform as an eluent. As shown in Figure 1, thermogravimetric analysis (TGA) indicates that the three conjugated polymers have good thermal stability with decomposition temperatures (with 5% weight loss) over ∼330 °C under a nitrogen atmosphere. Differential scanning calorimetry (DSC) showed that there was no obvious thermal transition up to 280 °C for all polymers. X-ray diffraction (XRD) also showed no clear diffraction peaks in the range of 2θ = 0−16°, indicating the amorphous nature of the three polymers (Figure S1).

Conformational Analysis by Density Functional Theory. Computational studies using density functional theory (DFT, B3LYP/6-31G** level) were performed (Figure 2).[25] With regard to crystalline **PTTBT14**, the most stable conformation was calculated to have a dihedral angle of ∼9° between the TT and BT moieties with attractive coulomb interactions through intrachain C−H···N and S···O interactions,[17,18,26−28] showing an almost planar structure. Similarly,

dx.doi.org/10.1021/am5061189 | ACS Appl. Mater. Interfaces 2014, 6, 20510−20518

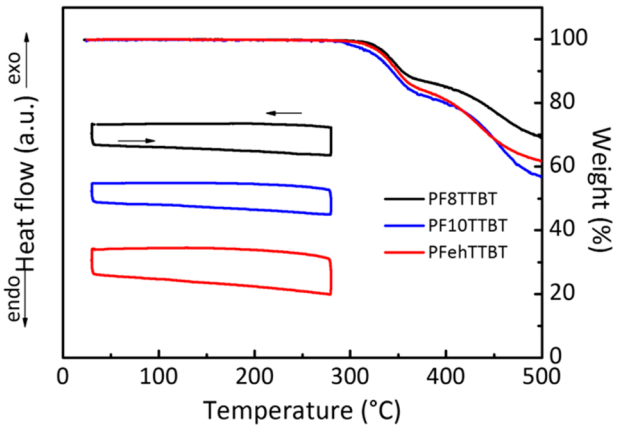

Figure 1. TGA and DSC thermograms for three polymers.

interchain coulomb interactions (as well as chain linearity and planarity) can increase the intermolecular organization, inducing a crystalline morphology. For the **PFTTBT** series, an almost planar conformation was also calculated with a torsion angle of ~25° between the fluorene and TT units and ~9° between the TT and BT moieties. The frontier orbitals (HOMO and LUMO) show similar structures for the two types of crystalline and amorphous TT-BT based polymers. The LUMO is concentrated mainly on the e-deficient BT and the HOMO is delocalized along the TT and BT units. The fluorene moiety contributes slightly to the HOMO, which can decrease the HOMO energy level relative to that of **PTTBT14**.[3,29] On the other hand, the incorporation of fluorene in the polymeric backbone might weaken the interchain ordering due to a disruption of the intra- and interchain attractive coulomb interactions. The noncovalent dipolar interactions work uniformly along the polymeric chain of **PTTBT14** but this uniformity is broken due to the absence of these attractive interactions around the fluorene moiety in the **PFTTBT** polymers, suggesting crystalline and amorphous characteristics for **PTTBT14** and **PFTTBT** polymers.

Optical and Electrochemical Properties. Figure 3 shows the UV−vis absorption spectra of the polymers in chloroform and in film. The three polymers showed similar spectra in chloroform. The spectra in solution showed two absorption bands in the range of 350−650 nm. The band at ~400 nm originates from the $\pi-\pi^*$ transition of the π-conjugated backbone and the peak at ~530 nm can be assigned to intramolecular charge transfer (ICT) band between the e-rich TT and e-poor BT moieties. In the film state, the absorption spectra of **PFTTBT** polymers were red-shifted slightly (by ca. 10−30 nm) due to interchain aggregation in the solid phase. The alkyl side chains on the fluorene unit have a substantial effect on the intermolecular organization. **PF8TTBT** with a linear octyl group showed a more red-shifted absorption maximum (λ_{abs} = 568 nm) in the film compared to those (λ_{abs} = 540−543 nm) of **PF10TTBT** and **PFehTTBT** with branched side chains, indicating that the bulky branched side chains disrupt the interchain organization. A similar optical bandgap was measured to be 1.93−1.96 eV for all polymers from the onset point in the film. In contrast, semicrystalline **PTTBT14** shows a pronounced shoulder peak (at 660 nm) in its UV−vis spectrum, even in the solution state, indicating significant interchain organization in both solution and in thin film form (bandgap 1.73 eV). This originates from the strong interchain

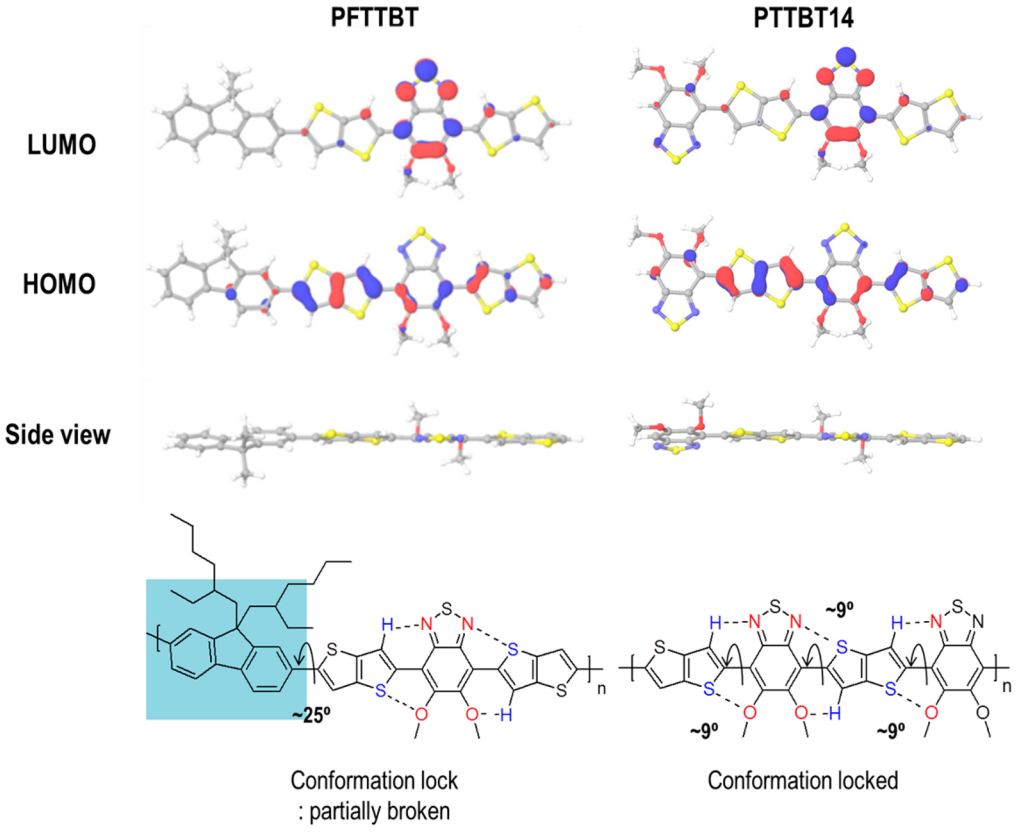

Figure 2. Frontier orbitals and the most stable conformations of **PFTTBT** and **PTTBT14** polymers.

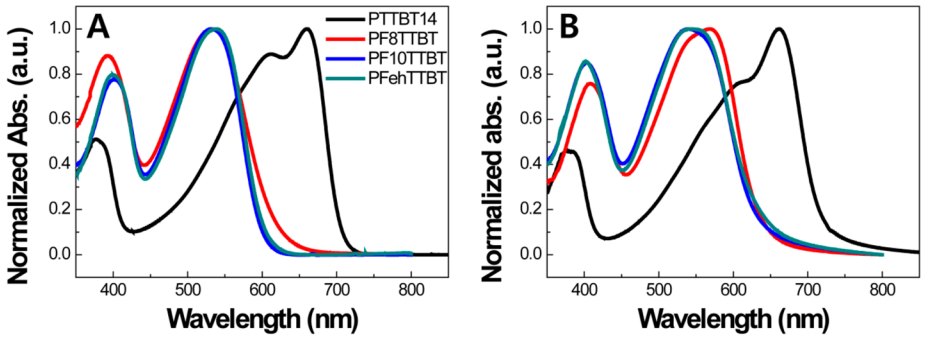

Figure 3. UV−vis absorption spectra of polymers (a) in chloroform and (b) in film. The spectra of **PTTBT14** were included for comparison with permission from Lee et al. (Reprinted from ref 14. Copyright 2014 American Chemical Society).

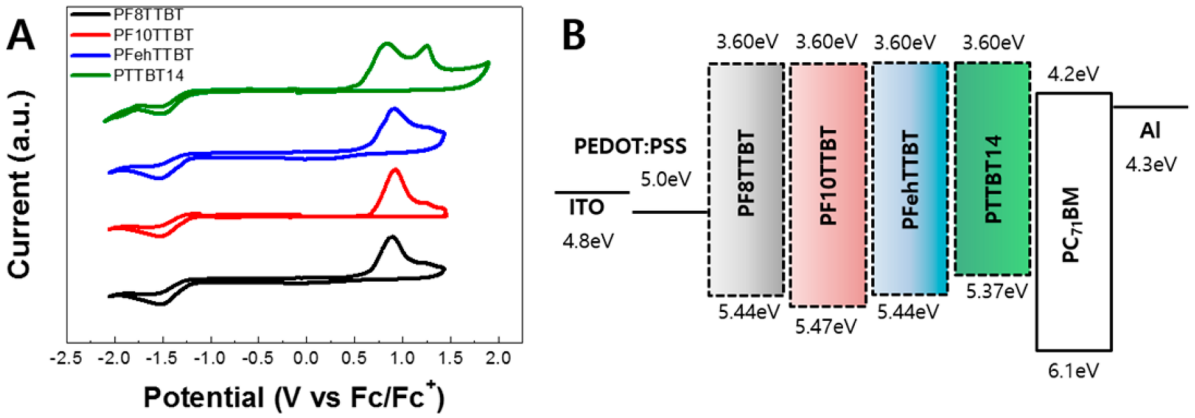

Figure 4. (a) Cyclic voltammograms of polymers and (b) resulting energy band diagram. The CV of PTTBT14 was included for comparison with permission from Lee et al. (Reprinted from ref 14. Copyright 2014 American Chemical Society).

Table 1. Optical and Electrochemical Properties of Polymers

				soln	film				
polymers	M_n[a] (g/mol)	PDI	T_d[b] (°C)	λ_{abs} (nm)[c]	λ_{abs} (nm)[d]	E_g^{opt} (eV)[e]	E_{HOMO}[f](eV)	E_{LUMO}[f] (eV)	E_g^{electg} (eV)
PF8TTBT	34000	2.8	339	532	568	1.96	−5.44	−3.60	1.84
PF10TTBT	44000	2.5	326	532	540	1.96	−5.47	−3.60	1.87
PFehTTBT	34000	2.3	333	537	543	1.93	−5.44	−3.60	1.84

[a]Number-average molecular weight. [b]Decomposition temperature (T_d) was determined by TGA (with 5% weight loss). [c]Dilute solution in chloroform. [d]Spin-cast film on glass from 1 wt % chloroform solution for 30 s at 1500 rpm. [e]Optical bandgap calculated from the absorption edge in film. [f]HOMO and LUMO levels were determined by measuring onset potentials of the first oxidation (E_{ox}) and reduction (E_{red}) peaks relative to ferrocene (F_c), the ionization potential (IP) value of which is −4.8 eV for the F_c/F_c^+ redox system. [g]Electrochemical bandgap.

interactions owing to the rigid, planar, and linear chain structure of **PTTBT14** via intra- and/or interchain hydrogen bonds and dipole−dipole coulomb interactions.[30] The introduction of a fluorene unit into the polymeric backbone breaks up the chain linearity and planarity, and disrupts the crystalline intermolecular organization, leading to a large blue-shift in the spectra and an increase in bandgap compared to **PTTBT14**. The alkyl-substituents on the fluorene unit and the increased chain curvature might hinder interchain packing, causing the amorphous character of the resulting polymers. The largely blue-shifted featureless spectra without shoulder peaks clearly support the amorphous nature of the polymers by incorporating the alkyl-substituted fluorene moiety in the polymer chain.

The electrochemical properties were examined by cyclic voltammetry (CV) for the three polymers. Figure 4 shows the cyclic voltammograms, and Table 1 lists the data. All the **PFTTBT** polymers showed irreversible oxidation and reduction peaks. The HOMO and LUMO energy levels were calculated from the oxidation and reduction onset potentials relative to ferrocene as the internal standard. The HOMO energy levels (−5.44 to −5.47 eV) of the **PFTTBT** polymers were down-shifted substantially compared to that (−5.37 eV) of **PTTBT14**, due to the significant decrease in interchain packing and effective conjugation by the presence of the fluorene moiety. The three **PFTTBT** polymers showed similar HOMO and LUMO values and the alkyl substituents did not have a significant influence on the frontier orbitals. Considering that the LUMO level of $PC_{71}BM$ is −4.2 eV, the energy offsets between the **PFTTBT** polymers and the acceptor $PC_{71}BM$ are in the range of ∼0.6 eV, from which efficient exciton dissociation is expected. The deeper HOMO of the **PFTTBT** structures is also expected to increase the V_{OC} compared to **PTTBT14**. Table 1 summarizes the physical, optical, thermal, and electrochemical properties of the polymers.

Photovoltaic Properties. Polymeric solar cell (PSC) devices were fabricated with the following device configuration: ITO/PEDOT:PSS/polymers:$PC_{71}BM$/LiF/Al. The thickness of the PEDOT:PSS, LiF, and Al layer was approximately 40, 1, and 100 nm, respectively. Photovoltaic devices were fabricated by blending polymers with $PC_{71}BM$ in *o*-dichlorobenzene (ODCB). To optimize the device fabrication condition, the devices were tested by varying the blend ratio, thermal treatments, and processing additives, etc. The best performing devices were obtained with the blends of polymer:$PC_{71}BM$ = 1:4 (by weight) in ODCB (40 mg/mL) for the three **PFTTBT** polymers. A previous study on **PTTBT14** revealed the maximum PCE (2.4–2.6%) with the blend film of polymer:$PC_{61}BM$ = 1:1 (by weight).[14] The optimal blend ratio is clearly different for the crystalline **PTTBT14** and amorphous **PFTTBT** polymers. The intercalation of fullerene derivatives into the polymer domain normally determines the optimal polymer:fullerene mixing ratio. In the case of amorphous photovoltaic polymers, the intercalation of fullerenes occurs effectively between the polymer side-chains, resulting in a higher content of fullerenes needed to form an electron-transporting fullerene phase.[31] The insufficient fullerene content in the blended film leads to inefficient charge separation and electron transporting properties. Mayer et al. characterized the number of fullerenes per repeating polymer unit in the intercalated phase and suggested that this ratio is important for determining the optimal blend ratio.[32]

Figure 5 shows the typical current density–voltage (J–V) curves of PSCs under AM 1.5G solar radiation (100 mW/cm^2).

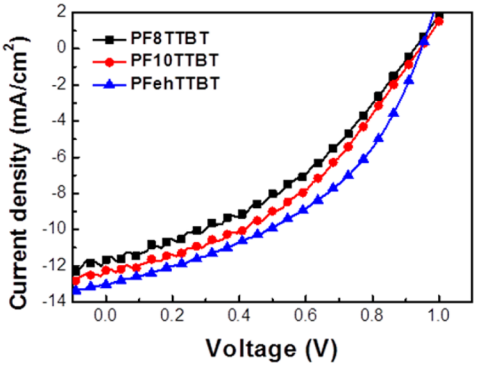

Figure 5. Current density–voltage (J–V) characteristics of **PFTTBT**:$PC_{71}BM$ PSCs.

Table 2 lists the detailed photovoltaic parameters. The incorporation of alkyl-substituted fluorene moieties endowed the **PFTTBT** polymers with better solubility in chlorinated solvents than **PTTBT14**, and the photovoltaic characteristics also improved substantially, showing 4.2–5.3% PCEs. **PF8TTBT** with linear octyl substituents showed a 4.2% PCE with a V_{OC} of 0.92 V, J_{SC} of 11.7 mA/cm^2, and FF of 0.39. The branched alkyl substituted **PF10TTBT** and **PFehTTBT** photovoltaic devices showed PCE values of 4.7% and 5.3% with a V_{OC} of 0.94 and 0.95 V, J_{SC} of 12.3 and 13.0 mA/cm^2, and FF of 0.41 and 0.43, respectively. Compared to the crystalline **PTTBT14** device (Table 2), the V_{OC} and J_{SC} values improved substantially and the resulting PCE increased significantly. The larger V_{OC} is understood in terms of the deeper HOMO of the **PFTTBTs** (−5.44 to −5.47 eV for **PFTTBTs** vs −5.37 eV for **PTTBT14**). Interestingly, the amorphous **PFTTBT** polymers showed noticeably high J_{SC} (up to ~15 mA/cm^2) despite the larger bandgap (~1.9 eV) and low hole mobility of 9.63×10^{-7} to 7.45×10^{-6} cm^2/(V s) (Figure S2). The increased J_{SC} is expected to be related closely to the film morphology. The morphology of polymer/$PC_{71}BM$ (1:4 by weight) blend films was examined by tapping mode atomic force microscopy (AFM) and transmission electron microscopy (TEM) (Figure 6). The blended films showed no serious phase segregation (indicating homogeneous intermixing of polymer and $PC_{71}BM$) and very smooth surfaces with a root mean-square (rms) roughness of 0.4–0.5 nm. In both the TEM and AFM images, the bulky ethylhexyl side chains in **PFehTTBT** induce a more featureless and homogeneous morphology compared to the other polymers, possibly due to the more amorphous nature. This homogeneously intermixed morphology of **PFehTTBT**:$PC_{71}BM$ may improve a probability of exciton dissociation, resulting in enhanced J_{SC} and PCE. In contrast, the **PTTBT14** blended film had a highly ordered morphology with large crystalline domains according to GIWAXS (well resolved reflection peaks up to (300) along the q_z direction, interlamellar spacing = ~23 Å) and AFM (rms roughness = 1.21 nm) measurements.[14] This material showed poor miscibility with $PC_{61}BM$ due to the strong self-organizing properties of the crystalline polymer.[14,33,34] The excessively strong self-interactions among the crystalline polymers might hinder the formation of interpenetrating bicontinuous networks with fullerene acceptors, which is essential to achieving highly efficient photovoltaic performance. Despite the large V_{OC} and J_{SC} in the **PFTTBT** solar cells, the main drawback of the amorphous **PFTTBT** devices was found to be the poor FF value (0.39–0.48), probably due to the poor charge carrier mobility and imbalance in the electron/hole mobility ratio with the resulting geminate and nongeminate charge recombination. The FF is limited by the low exciton dissociation or transport of carriers in the low mobility regime.[35] Carriers with lower mobility may accumulate in the device, inducing an extra electric field that can block the same type of carrier drifting to the electrode under the built-in potential. This reduces the shunt resistance (R_{sh}) and FF.[35,36] The hole/electron mobility ratio was measured to be of μ_h/μ_e = 6.7, 0.55, and 1.03 for **PF8TTBT**:$PC_{71}BM$, **PF10TTBT**:$PC_{71}BM$, and **PFehTTBT**:$PC_{71}BM$, respectively. Among three polymers, **PFehTTBT**:$PC_{71}BM$ showed a well-balanced hole/electron

Table 2. Photovoltaic Parameters under AM1.5G (100 mW/cm^2)

donor:acceptor (blend ratio)	condition	solar cell parameters V_{oc} (V)	J_{sc} (mA/cm^2)	FF	PCE (%)
PF8TTBT:$PC_{71}BM$ (1:4)	no additive	0.92	11.7	0.39	4.2
	DIO 2%	0.91	12.8	0.39	4.5
PF10TTBT:$PC_{71}BM$ (1:4)	no additive	0.94	12.3	0.41	4.7
	DIO 2%	0.94	13.1	0.45	5.5
PFehTTBT:$PC_{71}BM$ (1:4)	no additive	0.95	13.0	0.43	5.3
	DIO 2%	0.94	13.3	0.44	5.5
	TiOx layer	0.92	15.1	0.48	6.6
PTTBT14:$PC_{61}BM$ (1:1)[14]	no additive	0.77	5.49	0.57	2.4
	ODT 2%[a]	0.74	7.00	0.51	2.6

[a]ODT: 1,8-octanedithiol.

dx.doi.org/10.1021/am5061189 | ACS Appl. Mater. Interfaces 2014, 6, 20510–20518

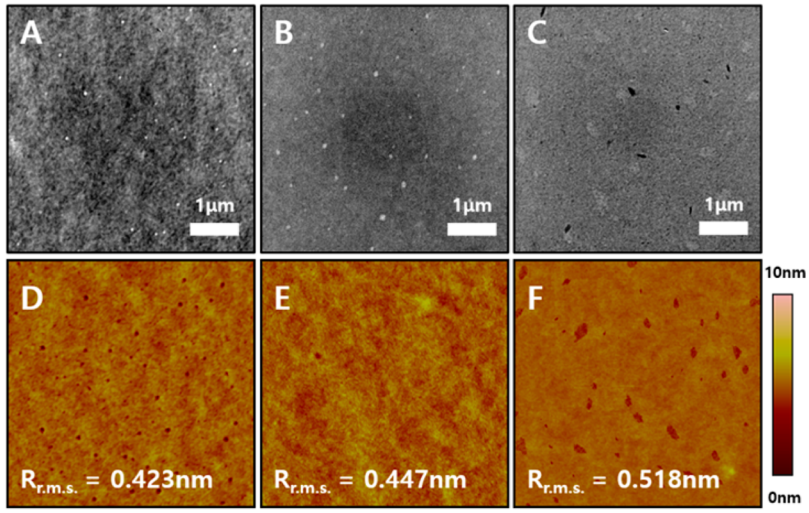

Figure 6. (a–c) TEM and (d–f) AFM topography images of (a, d) **PF8TTBT**, (b, e) **PF10TTBT**, and (c, f) **PFehTTBT** blend films (polymer:$PC_{71}BM$ = 1:4 by weight).

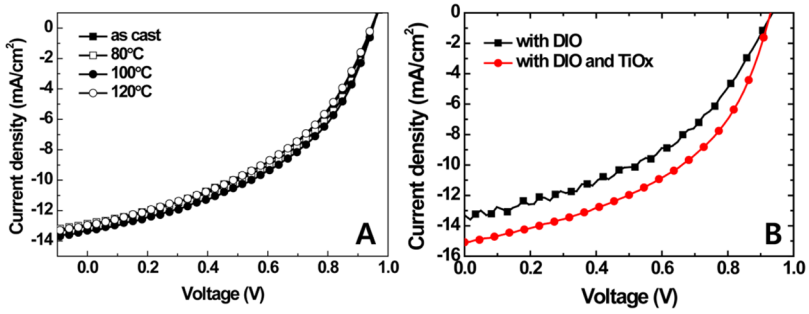

Figure 7. (a) Current density–voltage (J–V) characteristics of **PFehTTBT**:$PC_{71}BM$ with changing annealing temperatures. (b) J–V curves of **PFehTTBT**:$PC_{71}BM$ with DIO as a solvent additive and TiOx layer as an optical spacer.

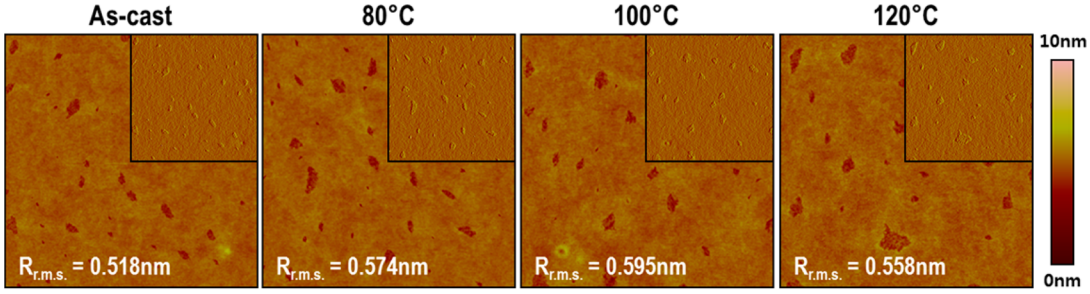

Figure 8. AFM surface topography images of **PFehTTBT**:$PC_{71}BM$ (1:4 by weight) blend films with increasing annealing temperatures (inset: phase images). Image size: 5 μm × 5 μm.

mobility ratio, showing the highest J_{SC} and *FF* values. (Figure S2).

To further improve the device properties, the **PFehTTBT** solar cells were treated thermally by changing the annealing temperature up to 120 °C. The photovoltaic parameters were measured together with the film morphology by AFM. No noticeable changes or improvements in the J–V characteristics (Figure 7) and AFM surface morphologies (Figure 8) were observed. A similar trend was noted for the linear alkyl substituted **PF8TTBT** (Figure S3), which is closely related to the amorphous nature of the **PFTTBT** polymers.

Processing additives might offer an effective way of optimizing the film morphology of the active layer. Several additives were tested to modulate the morphology of the blended films. Upon the addition of 2 vol % 1,8-diiodooctane (DIO) as a processing additive, the photovoltaic properties of **PFTTBT**:$PC_{71}BM$ PSCs were improved, showing PCEs in the range, 4.5–5.5% (Table 22). However, the processing additive effect was not significant. The AFM data showed the disappearance of pin holes in the film with DIO, resulting in a smoother surface with no clear changes (Figure S4).[37] With regard to the semicrystalline polymers, a clear additive effect has often been reported, where the solvent additive solvates one of the components in BHJ PSCs, facilitating intermolecular ordering in the donor and/or acceptor domains. Upon treatment with the solvent additives for semicrystalline structures, clear morphological changes (surface roughness and domain size, etc.) were also observed in the AFM images

with the appearance of a well-resolved interlamellar scattering peak with cofacial $\pi-\pi$ stacking in the GIWAXS measurements.[8,19,38,39] This shows a clear difference with the amorphous **PFTTBT** polymers. As shown in Figure 7, the incorporation of a TiOx layer as an optical spacer maximized the PCE to 6.6% without any noticeable changes in the surface morphology. The TiOx layer was reported to improve the photogeneration of charge carriers in the ITO/PEDOT:PSS/P3HT:$PC_{61}BM$/TiOx/Al device with an increased J_{SC} (by ~50%) by an optical interference effect with a spatial redistribution of the light intensity.[40]

CONCLUSIONS

We synthesized new amorphous thienothiophene (TT)-benzothiadiazole (BT) based conjugated polymers and studied their optical, electrochemical, morphological, and photovoltaic properties by comparing with those of a crystalline polymer. Recently, the charge carrier transport and photovoltaic characteristics of a highly crystalline TT-BT based copolymer (**PTTBT14**) were reported. Although crystalline **PTTBT14** showed significantly high hole mobility (0.26 $cm^2/(V\ s)$), its photovoltaic properties were poor, showing a PCE of 2.4–2.6%. A linear **PTTBT14** showed excessively strong self-interactions and little miscibility with $PC_{61}BM$, suggesting that the high crystallinity of a photoactive polymer does not always guarantee a high PCE. Here, the alkyl-substituted fluorene was incorporated in the linear and rigid TT-BT backbone to disrupt the conformational lock and intermolecular coulomb interactions. The resulting **PFTTBT** polymers showed an amorphous nature with a deeper HOMO, wider bandgap, better solution processability, good miscibility with fullerene moieties, and considerably improved photovoltaic characteristics compared to **PTTBT14**. The optimized photovoltaic device exhibited a PCE of 6.6% with a V_{OC} of 0.92 V, a J_{SC} of 15.1 mA/cm^2, and an FF of 0.48. The V_{OC} and J_{SC} values of the amorphous PSCs were quite promising but the low FF was found to be the main drawback. The poor FF is related mainly to poor interchain ordering, the resulting low carrier mobility and increased geminate and nongeminate charge recombination. In addition, the optimized PSCs were obtained with excess fullerene acceptors (polymer:$PC_{71}BM$ blend ratio of 1:4) where negligible effects were measured by thermal annealing. Based on this study, we suggest that the crystalline (or amorphous) nature of photovoltaic polymers can be fine-tuned (or adjusted) by the incorporation of the third moiety in the D–A type copolymer. To further optimize the OPVs, it is desirable to fully utilize the advantages of both crystalline and amorphous structures. By incorporating and adjusting the third moiety (molecular structure and feed ratio) in the crystalline D–A polymeric backbone, it is possible to partially disrupt the intra- and interchain organizations to finely control intermolecular ordering and the morphological properties (i.e., miscibility with fullerene derivatives) for maximizing the photovoltaic characteristics.

ASSOCIATED CONTENT

Supporting Information

X-ray diffraction data, AFM images, ^1H NMR spectra, and $J-V$ curves of electron- and hole-only devices by an SCLC technique. This material is available free of charge via the Internet at http://pubs.acs.org.

AUTHOR INFORMATION

Corresponding Authors

*E-mail: cep@postech.ac.kr (C.E.P.).
*E-mail: hywoo@pusan.ac.kr (H.Y.W.).

Author Contributions

§W.L. and H.C. contributed equally.

Notes

The authors declare no competing financial interest.

ACKNOWLEDGMENTS

This study was supported by the National Research Foundation (NRF) Grant, Korea (2012R1A1A2005855, 2012M3A6A7055540, 2011-0031639). This work was supported by the New & Renewable Energy Core Technology Program of the Korea Institute of Energy Technology Evaluation and Planning (KETEP), granted financial resource from the Ministry of Trade, Industry & Energy, Republic of Korea (No. 20133030011330). Synchrotron X-ray scattering measurements at Pohang Accelerator Laboratory were supported by MEST, POSCO, and the POSTECH Foundation. We also thank The Center for Advanced Soft Electronics under the Global Frontier Research Program (Nos. 20110031639) through the National Research Foundation funded by the Ministry of Education, Science and Technology (Korea).

REFERENCES

(1) Zhou, H. X.; Yang, L. Q.; You, W. Rational Design of High Performance Conjugated Polymers for Organic Solar Cells. *Macromolecules* **2012**, *45*, 607–632.

(2) Son, H. J.; He, F.; Carsten, B.; Yu, L. P. Are We There Yet? Design of Better Conjugated Polymers for Polymer Solar Cells. *J. Mater. Chem.* **2011**, *21*, 18934–18945.

(3) Cheng, Y. J.; Yang, S. H.; Hsu, C. S. Synthesis of Conjugated Polymers for Organic Solar Cell Applications. *Chem. Rev.* **2009**, *109*, 5868–5923.

(4) Kang, T. E.; Kim, K.-H.; Kim, B. J. Design of Terpolymers as Electron Donors for Highly Efficient Polymer Solar Cells. *J. Mater. Chem. A* **2014**, *2*, 15252–15267.

(5) Thompson, B. C.; Fréchet, J. M. J. Polymer–Fullerene Composite Solar Cells. *Angew. Chem., Int. Ed.* **2008**, *47*, 58–77.

(6) Liu, S. J.; Zhang, K.; Lu, J. M.; Zhang, J.; Yip, H. L.; Huang, F.; Cao, Y. High-Efficiency Polymer Solar Cells via the Incorporation of an Amino-Functionalized Conjugated Metallopolymer as a Cathode Interlayer. *J. Am. Chem. Soc.* **2013**, *135*, 15326–15329.

(7) He, Z. C.; Zhong, C. M.; Su, S. J.; Xu, M.; Wu, H. B.; Cao, Y. Enhanced Power-Conversion Efficiency in Polymer Solar Cells Using an Inverted Device Structure. *Nat. Photonics* **2012**, *6*, 591–595.

(8) Nguyen, T. L.; Choi, H.; Ko, S. J.; Uddin, M. A.; Walker, B.; Yum, S.; Jeong, J. E.; Yun, M. H.; Shin, T. J.; Hwang, S.; Kim, J. Y.; Woo, H. Y. Semi-Crystalline Photovoltaic Polymers with Efficiency Exceeding 9% in a 300 nm Thick Conventional Single-Cell Device. *Energy Environ. Sci.* **2014**, *7*, 3040–3051.

(9) You, J. B.; Dou, L. T.; Yoshimura, K.; Kato, T.; Ohya, K.; Moriarty, T.; Emery, K.; Chen, C. C.; Gao, J.; Li, G.; Yang, Y. A Polymer Tandem Solar Cell with 10.6% Power Conversion Efficiency. *Nat. Commun.* **2013**, *4*, 1446–1455.

(10) Li, C.-Z.; Chang, C.-Y.; Zang, Y.; Ju, H.-X.; Chueh, C.-C.; Liang, P.-W.; Cho, N.; Ginger, D. S.; Jen, A. K. Y. Suppressed Charge Recombination in Inverted Organic Photovoltaics via Enhanced Charge Extraction by Using a Conductive Fullerene Electron Transport Layer. *Adv. Mater.* **2014**, *26*, 6262–6267.

(11) Zhang, S.; Ye, L.; Zhao, W.; Liu, D.; Yao, H.; Hou, J. Side Chain Selection for Designing Highly Efficient Photovoltaic Polymers with 2D-Conjugated Structure. *Macromolecules* **2014**, *47*, 4653–4659.

(12) Ajayaghosh, A. Donor-Acceptor Type Low Band Gap Polymers: Polysquaraines and Related Systems. *Chem. Soc. Rev.* **2003**, *32*, 181−191.
(13) Jung, I. H.; Yu, J.; Jeong, E.; Kim, J.; Kwon, S.; Kong, H.; Lee, K.; Woo, H. Y.; Shim, H. K. Synthesis and Photovoltaic Properties of Cyclopentadithiophene-Based Low-Bandgap Copolymers That Contain Electron-Withdrawing Thiazole Derivatives. *Chem.—Eur. J.* **2010**, *16*, 3743−3752.
(14) Lee, W.; Kim, G.-H.; Ko, S.-J.; Yum, S.; Hwang, S.; Cho, S.; Shin, Y.-H.; Kim, J. Y.; Woo, H. Y. Semicrystalline D−A Copolymers with Different Chain Curvature for Applications in Polymer Optoelectronic Devices. *Macromolecules* **2014**, *47*, 1604−1612.
(15) Biniek, L.; Fall, S.; Chochos, C. L.; Leclerc, N.; Leveque, P.; Heiser, T. Optimization of the Side-Chain Density to Improve the Charge Transport and Photovoltaic Performances of a Low Band Gap Copolymer. *Org. Electron.* **2012**, *13*, 114−120.
(16) Wang, X. C.; Sun, Y. P.; Chen, S.; Guo, X.; Zhang, M. J.; Li, X. Y.; Li, Y. F.; Wang, H. Q. Effects of pi-Conjugated Bridges on Photovoltaic Properties of Donor-pi-Acceptor Conjugated Copolymers. *Macromolecules* **2012**, *45*, 1208−1216.
(17) Jackson, N. E.; Savoie, B. M.; Kohlstedt, K. L.; de la Cruz, M. O.; Schatz, G. C.; Chen, L. X.; Ratner, M. A. Controlling Conformations of Conjugated Polymers and Small Molecules: The Role of Nonbonding Interactions. *J. Am. Chem. Soc.* **2013**, *135*, 10475−10483.
(18) Guo, X. G.; Quinn, J.; Chen, Z. H.; Usta, H.; Zheng, Y.; Xia, Y.; Hennek, J. W.; Ortiz, R. P.; Marks, T. J.; Facchetti, A. Dialkoxybithiazole: A New Building Block for Head-to-Head Polymer Semiconductors. *J. Am. Chem. Soc.* **2013**, *135*, 1986−1996.
(19) Lee, W.; Choi, H.; Hwang, S.; Kim, J. Y.; Woo, H. Y. Efficient Conventional- and Inverted-Type Photovoltaic Cells Using a Planar Alternating Polythiophene Copolymer. *Chem.—Eur. J.* **2012**, *18*, 2551−2558.
(20) Rieger, R.; Beckmann, D.; Mavrinskiy, A.; Kastler, M.; Müllen, K. Backbone Curvature in Polythiophenes. *Chem. Mater.* **2010**, *22*, 5314−5318.
(21) Lei, T.; Cao, Y.; Zhou, X.; Peng, Y.; Bian, J.; Pei, J. Systematic Investigation of Isoindigo-Based Polymeric Field-Effect Transistors: Design Strategy and Impact of Polymer Symmetry and Backbone Curvature. *Chem. Mater.* **2012**, *24*, 1762−1770.
(22) Guo, Z.; Lee, D.; Schaller, R. D.; Zuo, X.; Lee, B.; Luo, T.; Gao, H.; Huang, L. Relationship between Interchain Interaction, Exciton Delocalization, and Charge Separation in Low-Bandgap Copolymer Blends. *J. Am. Chem. Soc.* **2014**, *136*, 10024−10032.
(23) Jo, J.; Chi, C.; Höger, S.; Wegner, G.; Yoon, D. Y. Synthesis and Characterization of Monodisperse Oligofluorenes. *Chem.—Eur. J.* **2004**, *10*, 2681−2688.
(24) Mihailetchi, V. D.; Wildeman, J.; Blom, P. W. M. Space-Charge Limited Photocurrent. *Phys. Rev. Lett.* **2005**, *94*, 126602.
(25) Zhou, H. X.; Yang, L. Q.; Xiao, S. Q.; Liu, S. B.; You, W. Donor-Acceptor Polymers Incorporating Alkylated Dithienylbenzothiadiazole for Bulk Heterojunction Solar Cells: Pronounced Effect of Positioning Alkyl Chains. *Macromolecules* **2010**, *43*, 811−820.
(26) Zotti, G.; Gallazzi, M. C.; Zerbi, G.; Meille, S. V. Conducting Polymers from Anodic Coupling of Some Regiochemically Defined Dialkoxy-Substituted Thiophene Oligomers. *Synth. Met.* **1995**, *73*, 217−225.
(27) Meille, S. V.; Farina, A.; Bezziccheri, F.; Gallazzi, M. C. The Influence of Alkoxy Side-Chains on the Conformational Flexibility of Oligothiophenes and Polythiophenes. *Adv. Mater.* **1994**, *6*, 848−851.
(28) Wang, Y. F.; Parkin, S. R.; Gierschner, J.; Watson, M. D. Highly Fluorinated Benzobisbenzothiophenes. *Org. Lett.* **2008**, *10*, 3307−3310.
(29) Kong, H.; Lee, D. H.; Kang, I. N.; Lim, E.; Jung, Y. K.; Park, J. H.; Ahn, T.; Yi, M. H.; Park, C. E.; Shim, H. K. New Amorphous Semiconducting Copolymers Containing Fluorene and Thiophene Moieties for Organic Thin-Film Transistors. *J. Mater. Chem.* **2008**, *18*, 1895−1902.
(30) Peet, J.; Cho, N. S.; Lee, S. K.; Bazan, G. C. Transition from Solution to the Solid State in Polymer Solar Cells Cast from Mixed Solvents. *Macromolecules* **2008**, *41*, 8655−8659.
(31) Cates, N. C.; Gysel, R.; Beiley, Z.; Miller, C. E.; Toney, M. F.; Heeney, M.; McCulloch, I.; McGehee, M. D. Tuning the Properties of Polymer Bulk Heterojunction Solar Cells by Adjusting Fullerene Size to Control Intercalation. *Nano Lett.* **2009**, *9*, 4153−4157.
(32) Mayer, A. C.; Toney, M. F.; Scully, S. R.; Rivnay, J.; Brabec, C. J.; Scharber, M.; Koppe, M.; Heeney, M.; McCulloch, I.; McGehee, M. D. Bimolecular Crystals of Fullerenes in Conjugated Polymers and the Implications of Molecular Mixing for Solar Cells. *Adv. Funct. Mater.* **2009**, *19*, 1173−1179.
(33) Moule, A. J.; Allard, S.; Kronenberg, N. M.; Tsami, A.; Scherf, U.; Meerholz, K. Effect of Polymer Nanoparticle Formation on the Efficiency of Polythiophene Based "Bulk-Heterojunction" Solar Cells. *J. Phys. Chem. C* **2008**, *112*, 12583−12589.
(34) Moulé, A. J.; Meerholz, K. Morphology Control in Solution-Processed Bulk-Heterojunction Solar Cell Mixtures. *Adv. Funct. Mater.* **2009**, *19*, 3028−3036.
(35) Qi, B. Y.; Wang, J. Z. Fill Factor in Organic Solar Cells. *Phys. Chem. Chem. Phys.* **2013**, *15*, 8972−8982.
(36) Credgington, D.; Hamilton, R.; Atienzar, P.; Nelson, J.; Durrant, J. R. Non-Geminate Recombination as the Primary Determinant of Open-Circuit Voltage in Polythiophene:Fullerene Blend Solar Cells: an Analysis of the Influence of Device Processing Conditions. *Adv. Funct. Mater.* **2011**, *21*, 2744−2753.
(37) Cha, H.; Lee, G. Y.; Fu, Y.; Kim, Y. J.; Park, C. E.; Park, T. Simultaneously Grasping and Self-Organizing Photoactive Polymers for Highly Reproducible Organic Solar Cells with Improved Efficiency. *Adv. Energy Mater.* **2013**, *3*, 1018−1024.
(38) Peet, J.; Kim, J. Y.; Coates, N. E.; Ma, W. L.; Moses, D.; Heeger, A. J.; Bazan, G. C. Efficiency Enhancement in Low-Bandgap Polymer Solar Cells by Processing with Alkane Dithiols. *Nat. Mater.* **2007**, *6*, 497−500.
(39) Li, G.; Shrotriya, V.; Huang, J.; Yao, Y.; Moriarty, T.; Emery, K.; Yang, Y. High-Efficiency Solution Processable Polymer Photovoltaic Cells by Self-Organization of Polymer Blends. *Nat. Mater.* **2005**, *4*, 864−868.
(40) Kim, J. Y.; Kim, S. H.; Lee, H. H.; Lee, K.; Ma, W.; Gong, X.; Heeger, A. J. New Architecture for High-Efficiency Polymer Photovoltaic Cells Using Solution-Based Titanium Oxide as an Optical Spacer. *Adv. Mater.* **2006**, *18*, 572−576.